# Quantum Tricritical Points in NbFe$_2$

Sven Friedemann,[1,2] Will J. Duncan,[3] Max Hirschberger,[2,4,∗]

Thomas Bauer,[5] Robert Küchler,[5] Andreas Neubauer,[4]

Manuel Brando,[5] Christian Pfleiderer,[6] and F. Malte Grosche[2]

[1]*HH Wills Laboratory, University of Bristol, Bristol BS8 1TL, UK*

[2]*Cavendish Laboratory, University of Cambridge, Cambridge CB3 0HE, UK*

[3]*Department of Physics, Royal Holloway,*

*University of London, Egham TW20 0EX, UK*

[4]*Physik Department, Technische Universität München,*

*James Franck Straße, 85748 Garching, Germany*

[5]*MPI-CPfS, Nöthnitzer Strasse, 01189 Dresden, Germany*

[6]*Physik Department E21, Technische Universität München,*

*James Franck Straße, 85748 Garching, Germany*

(Dated: September 18, 2017)

# Abstract

Quantum critical points (QCPs) emerge when a 2nd order phase transition is suppressed to zero temperature. In metals the quantum fluctuations at such a QCP can give rise to new phases including unconventional superconductivity. Whereas antiferromagnetic QCPs have been studied in considerable detail ferromagnetic (FM) QCPs are much harder to access[1, 2]. In almost all metals FM QCPs are avoided through either a change to 1st order transitions or through an intervening spin-density-wave (SDW) phase. Here, we study the prototype of the second case, $NbFe_2$. We demonstrate that the phase diagram can be modelled using a two-order-parameter theory in which the putative FM QCP is buried within a SDW phase. We establish the presence of quantum tricritical points (QTCPs) at which both the uniform and finite $q$ susceptibility diverge. The universal nature of our model suggests that such QTCPs arise naturally from the interplay between SDW and FM order and exist generally near a buried FM QCP of this type. Our results promote $NbFe_2$ as the first example of a QTCP, which has been proposed as a key concept in a range of narrow-band metals, including the prominent heavy-fermion compound $YbRh_2Si_2$ [3].

---

\* Current address: Department of Physics, Princeton University, Jadwin Hall, Princeton NJ 08544, USA

Transition metal compounds with low-temperature magnetic order offer attractive departure points in the study of correlated electron materials. Key materials such as MnSi, $ZrZn_2$ or $Ni_3Al$ have been investigated for many years; high quality and well characterized single crystals are widely available, their magnetic states have been studied in detail, the magnetic excitation spectrum and their electronic structure are often known from neutron scattering and quantum oscillation measurements. A semi-quantitative understanding of key properties such as the size of the ordered moment, the ordering temperature and the low temperature heat capacity is achieved within spin fluctuation theory [4, 5]. Close to the border of magnetism, however, the predictions of conventional spin fluctuation theory no longer apply providing a long-standing fundamental challenge to our understanding of correlated electron systems [2]. Key discrepancies concern firstly, the low temperature form of the electrical resistivity $\rho(T)$, which follows a still insufficiently understood $T^{3/2}$ power-law temperature dependence on the paramagnetic side of the FM quantum phase transition [6–9] and secondly, the fate of ferromagnetic (FM) order itself: rather than being continuously suppressed towards a FM quantum critical point (QCP), the FM QCP is avoided in clean metals.

One scenario for the avoidance, by which the FM transition becomes 1st order near the putative QCP, is well understood by theory and experimentally well established [10–13]. The alternative scenario, namely that the FM QCP is masked – or buried – by emergent modulated magnetic order, has been discussed theoretically [14–17], but with the exception of early work on $NbFe_2$ [9, 18] and recent studies on $LaCrGe_3$ [19] as well as local moment systems PrPtAl [20], CeRuPO [21], CeFePO [22], and $YbRh_2Si_2$ [23] this second scenario has so far been little explored experimentally. Many of these materials bear the complication of additional energy scales from interactions between conduction electrons, localised $f$-electrons, crystal field levels, and complicated magnetic order. The transition metal itinerant magnet $NbFe_2$ avoids these complications and has a simple crystal and magnetic structure.

$NbFe_2$ can be tuned across a FM quantum phase transition by slight changes in the composition that preserve good crystal quality, enabling multi-probe studies without the complications of high pressure [9]. Whereas $Nb_{1-y}Fe_{2+y}$ orders ferromagnetically at low temperature for modest levels of iron excess $y > 0.01$, stoichiometric or Nb-rich $NbFe_2$ has long been known to exhibit signatures of a further magnetic phase transition [18, 24–26],

which has recently been proven by microscopic probes to tip the system into long-wavelength SDW order [27, 28]. The SDW transition temperature itself extrapolates smoothly to zero for $y \simeq -0.015$, and near this SDW QCP, the heat capacity Sommerfeld coefficient exhibits a logarithmic temperature dependence, whereas $\rho(T)$ follows a $T^{3/2}$ power-law form [9]. These prior findings strongly support the long-standing proposal [18] that a FM QCP is indeed buried within an emergent SDW phase in NbFe$_2$ and motivate a closer investigation. Here, we present detailed magnetic, electric transport and thermal expansion data collected in newly available high quality single crystals of the Nb$_{1-y}$Fe$_{2+y}$ system at key compositions in the phase diagram. We show that our data are consistent with a two-order-parameter Landau theory [29], which provides a novel and convenient framework for extracting robust findings, namely that (i) the avoided FM QCP can be located accurately inside the emergent SDW dome, (ii) the presence of SDW order causes the FM transition to become first order, and (iii) quantum tricritical points (QTCPs) emerge at finite field. Both SDW and FM fluctuations associated with the FM QTCPs will contribute to the excitation spectrum near the SDW QCP, which may explain the seemingly contradictory temperature dependencies of the heat capacity and resistivity in NbFe$_2$ mentioned above. Thus our results provide new routes towards understanding the enigmatic physics of materials at the border of ferromagnetism.

## I.  RESULTS

Our high-quality single crystals show the previously established variation of the FM and SDW phases in a set of zero-field measurements (Fig. 1). In iron-rich Nb$_{0.985}$Fe$_{2.015}$ signatures of both FM and SDW transitions are seen at $T_c \simeq 24\,\text{K}$ and $T_N \simeq 32\,\text{K}$, respectively as anomalies in the temperature dependent magnetic susceptibility $\chi(T)$, linear thermal expansion $\mathrm{d}L/(L_0 \mathrm{d}T)$ and electrical resistivity $\rho(T)$ (cf. Fig. 1). These signatures are consistent with 1st and 2nd order transitions at $T_c$ and $T_N$, respectively: The peak in $\chi(T)$ shows hysteresis at $T_c$ only, the thermal expansion shows a peak at $T_c$ and a kink at $T_N$, and the resistivity has a distinct kink at $T_c$ with hysteresis (Fig. S1), but only a much weaker anomaly is present in the derivative $\mathrm{d}\rho/\mathrm{d}T$ at $T_N$. The FM state is unambiguously identified by remanent magnetization (Fig. 3(a)).

Stoichiometric NbFe$_2$ displays a single transition at $T_N = 12\,\text{K}$ with the characteristics of
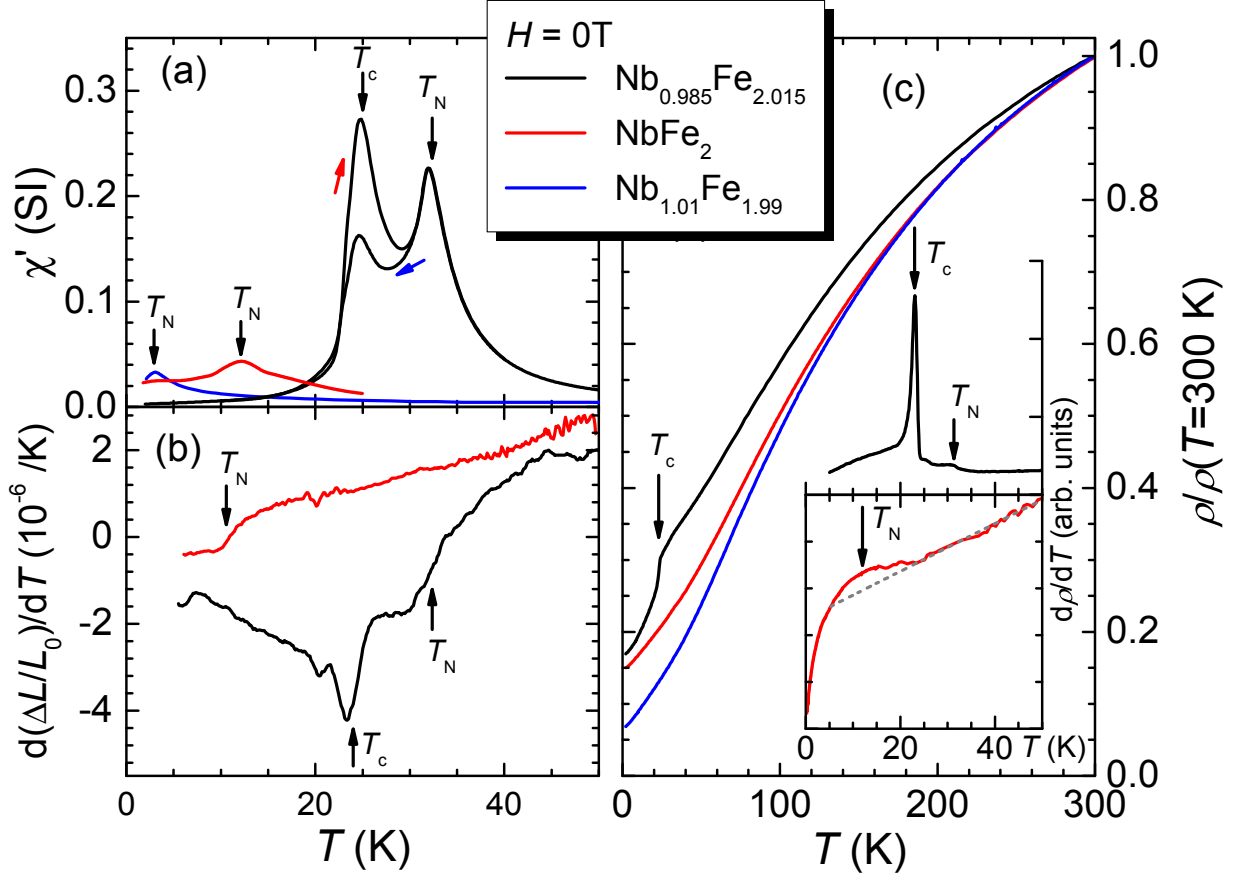
FIG. 1. Temperature dependence of the c-axis AC magnetic susceptibility $\chi(T)$ (a), the c-axis linear thermal expansion $\mathrm{d}L/(L_0\mathrm{d}T)$ (b), and of the electrical resistivity $\rho(T)$ (c) and its temperature derivative $\mathrm{d}\rho/\mathrm{d}T$ (inset in c) for $\mathrm{Nb}_{1-y}\mathrm{Fe}_{2+y}$ with $y = 0.015$ and $y = 0$. Vertical black arrows indicate the transitions at $T_\mathrm{c}$ and $T_\mathrm{N}$. Red and blue arrows in (a) indicate the measurement taken on warming and cooling.

SDW order: A peak in $\chi(T)$ without hysteresis, a kink in $\mathrm{d}L/(L\mathrm{d}T)$, and a weak enhancement in $\mathrm{d}\rho/\mathrm{d}T$ above the linear background from higher temperatures (Fig. 1). Similarly, for niobium rich $\mathrm{Nb}_{1.01}\mathrm{Fe}_{1.99}$, a single transition consistent with SDW order at $T_\mathrm{N} = 3\,\mathrm{K}$ can be inferred from the peak in $\chi(T)$ in Fig. 1(a).

The $H$-$T$ phase diagram is mapped for field parallel to the magnetic axis ($H \parallel c$) using magnetic susceptibility $\chi(T, H)$ measurements for a series of $\mathrm{Nb}_{1-y}\mathrm{Fe}_{2+y}$ samples spanning the range from FM ground state via samples with SDW ground state to those in ultimate proximity to the SDW QCP (Fig. 2). In iron-rich $\mathrm{Nb}_{0.985}\mathrm{Fe}_{2.015}$ the maxima in $\chi(T)$ signalling the 1st order ($T_\mathrm{c}$) and 2nd order ($T_\mathrm{N}$) transition shift to higher and lower temperature,
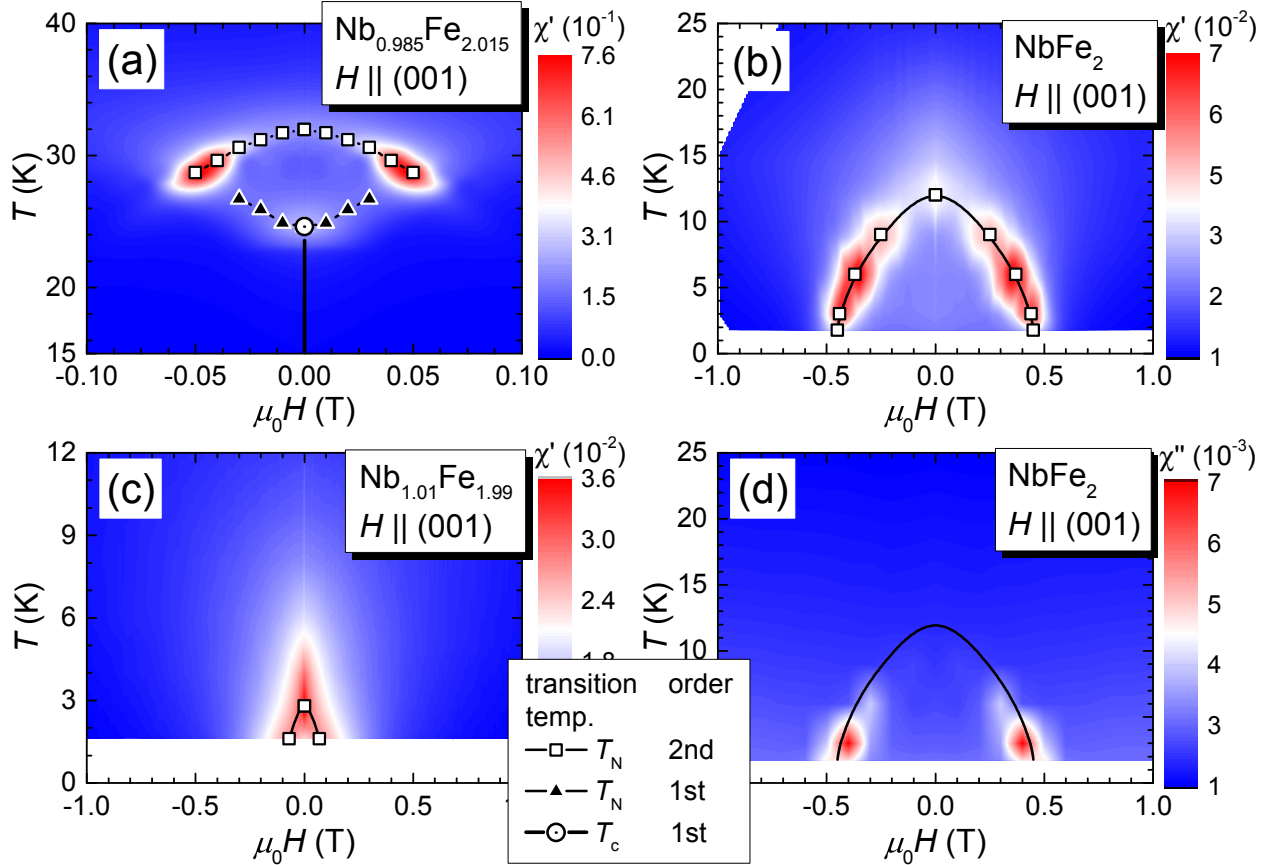
FIG. 2. Colour representation of the AC magnetic susceptibility $\chi(H, T)$ as a function of magnetic field and temperature for iron-rich $Nb_{0.985}Fe_{2.015}$ (a), stoichiometric $NbFe_2$ (b) and niobium-rich $Nb_{1.01}Fe_{1.99}$ (c). Points represent positions of the $\chi(T)$ maxima with (closed triangles) and without hysteresis (open squares) associated with $T_N$ as well as of the maximum in zero field (open circle) associated with $T_c$ (see text). (d) Imaginary part of the AC magnetic susceptibility $\chi''(H, T)$ for stoichiometric $NbFe_2$. Solid line in (d) marks the phase boundary from (b).

respectively for increasing magnetic field. The two signatures approach each other and eventually merge at a critical field $\mu_0 H^\star \simeq 0.06 \, \text{T}$ and a critical temperature $T^\star \simeq 28 \, \text{K}$. Only weak maxima reminiscent of crossovers are observed in $\chi(T)$ for fields above $H^\star$. Thus, the two lines of anomalies enclose the SDW phase which exists in the small parameter space between $T_N$ and $T_c$ and for fields $H \leq H^\star$ only. At the critical point $(H^\star, T^\star)$, the susceptibility reaches highest values comparable to those observed in band ferromagnets with a 2nd order transition near the Curie temperature, such as $ZrZn_2$, if slight inhomogeneity and demagnetizing fields are present. We will later see that this enhanced susceptibility is

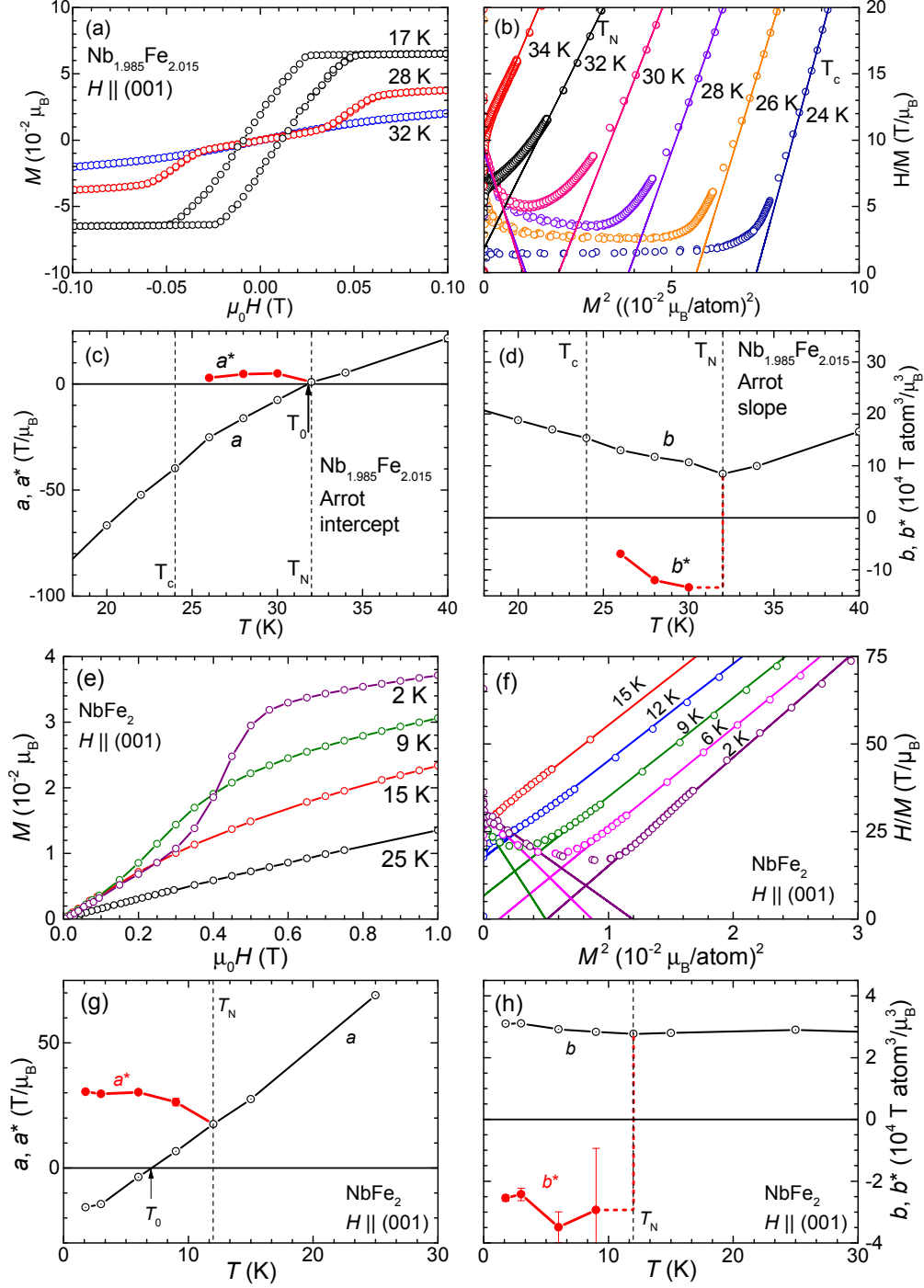FIG. 3. DC magnetization isotherms in iron-rich $Nb_{0.985}Fe_{2.015}$ (a) and stoichiometric $NbFe_2$ (e) for fields along the crystallographic $c$-direction. High and low-field straight-line fits to the Arrott plots of $H/M$ vs. $M^2$ (b, f) give intercepts $a$, $a^\star$ and slopes $b$, $b^\star$ for $Nb_{0.985}Fe_{2.015}$ (c, d) and $NbFe_2$ (g, h), enabling a direct comparison with a two order parameter Landau theory (see text).

expected within our model of competing order parameters and marks the tricritical point at the transition from first order to second order at $T^\star$ [30]. The 1st and 2nd order nature of the low-temperature and high-temperature boundary of the SDW phase can be inferred from the presence and absence of hysteresis in the AC susceptibility and electrical resistivity as detailed in Supplementary Material I.

In stoichiometric $NbFe_2$ the 2nd order transition can similarly be followed through the $H$-$T$ phase diagram: The maximum in $\chi(T)$ associated with $T_N$ is shifted to lower temperatures upon increasing the magnetic field up to a critical field of $H_N \approx 0.45\,T$. The line of anomalies separates out the low temperature, low field part of the $H$-$T$ phase diagram and suggests that in this region $NbFe_2$ forms a distinct broken-symmetry state. This "cap" for the SDW phase is reminiscent of the upper part of the SDW phase in iron-rich $Nb_{0.985}Fe_{2.015}$. In fact, we show below that the same competing order parameter model applies to both compositions and the phase diagram of stoichiometric $NbFe_2$ resembles that of iron-rich $Nb_{0.985}Fe_{2.015}$ with the temperature axis shifted down by $\approx 20\,K$.

Whilst the SDW transition remains 2nd order in $NbFe_2$ for most of the phase boundary, we find signatures of a tricritical point at $(H^\star = 0.44\,T, T^\star = 3\,K)$. Here, the susceptibility is strongly enhanced (Fig. 2(b) and S3) and a strong signal in the imaginary part $\chi''(H^\star, T^\star)$ is observed (Fig. 2(d)) like in iron-rich $Nb_{0.985}Fe_{2.015}$ at the tricritical point (cf. Supplementary Information I).

## II.  DISCUSSION

Identifying the lines of anomalies for $T < T^*$ as phase boundaries is uncontroversial, because they are associated with hysteresis. The case for a second order 'cap' linking the tricritical points at $(\pm H^\star, T^\star)$, however, needs to be examined carefully and is reminiscent of the situation in $Sr_3Ru_2O_7$ at high magnetic field. There, proof of a broken symmetry state (as opposed to metamagnetic transition lines ending in critical endpoints) came from thermal expansion and thermodynamic data [31]. In $NbFe_2$, further to earlier heat capacity measurements on polycrystals [18], strong support for the interpretation of the anomalies at $T_N$ as phase transition anomalies is provided by the thermal expansion shown in Fig. 1(b), as well as the observation of finite ordered moments within the SDW phase by ESR and $\mu SR$ studies [27].

Having established the presence of both the SDW and FM phase transitions we seek a consistent description of the low temperature phase diagram of $\mathrm{Nb}_{1-y}\mathrm{Fe}_{2+y}$ taking into account the proximity to both orders. At the most elementary level, this is done by postulating a Landau expansion of the free energy in terms of two order parameters [29]:

$$\frac{F}{\mu_0} = \frac{a}{2}M^2 + \frac{b}{4}M^4 + \frac{\alpha}{2}P^2 + \frac{\beta}{4}P^4 + \frac{\eta}{2}P^2M^2 - HM \qquad (1)$$

Here, $M$ denotes the uniform magnetization, which couples linearly to the applied magnetic field, whereas $P$ denotes a general second order parameter, which does not couple directly to the applied field but has a biquadratic coupling to the uniform magnetization. We associate the second order parameter $P$ with the SDW phase. The phenomenological parameters $a$ and $b$ can be extracted directly from magnetization measurements, for example $a = \chi^{-1}$ for $M = 0$, but the remaining parameters $\alpha$, $\beta$ and $\eta$ are more difficult to obtain. The theory can be formulated in terms of scalar order parameters in isotropic materials, because the more complicated coupling terms in a vector theory will constrain $M$ and $P$ either to point in the same direction or at right angles to each other [29]. In anisotropic materials, the situation is in principle more complicated, but as long as the field points along the easy axis as is the case for our studies of $\mathrm{Nb}_{1-y}\mathrm{Fe}_{2+y}$ here, the scalar description remains adequate.

In zero field the global free energy minima will correspond to either a paramagnetic state $M = P = 0$, or one of the possible magnetic states (i) $M = 0$, $P \neq 0$; (ii) $M \neq 0$, $P = 0$ or (iii) $M \neq 0$, $P \neq 0$, depending on the parameters $\{a, b, \alpha, \beta, \eta\}$. All prior observations in polycrystalline $\mathrm{NbFe}_2$, as well as our data on single crystals suggest that for $H = 0$ the mixed phase $M \neq 0$, $P \neq 0$ does not occur in $\mathrm{NbFe}_2$, and that on cooling the system will always first develop the SDW order parameter ($P \neq 0$), before that is replaced by a uniform magnetization. This constrains $\alpha(T)$ to go through zero at a higher temperature than $a(T)$. The expected phase diagram for this case is illustrated in Fig. 4.

We start by comparing the theoretical phase diagram with the observed behaviour in zero field: For $H = 0$ and within the $P \neq 0$ state the free energy has its global minimum at $F_P = -\alpha^2/(4\beta)$ for $P^2 = -\alpha/\beta$. However, if the system were to order uniformly, i.e. $M \neq 0$, the free energy would have a minimum of $F_M = -a^2/(4b)$ at $M^2 = -a/b$, and so a first order transition from the $M = 0$, $P \neq 0$ into the $M \neq 0$, $P = 0$ state will occur at a temperature $T_{\mathrm{c}}$, below which $a^2/b > \alpha^2/\beta$. This sequence of a 2nd order transition into

9

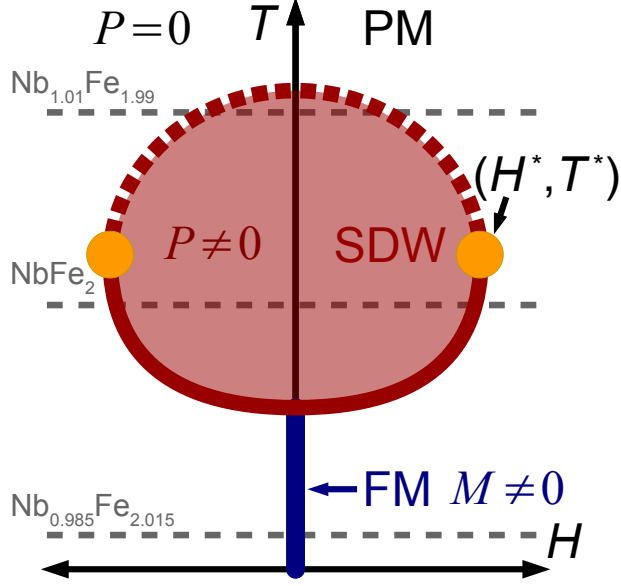FIG. 4. Schematic phase diagram based on the model free energy in Eqn. (1), as applied to $Nb_{1-y}Fe_{2+y}$. Solid blue and red lines indicate the first order phase boundaries of the SDW and FM phase. Dashed red lines indicate the 2nd order phase boundary of the SDW phase at high temperatures. Orange circles mark the tricritical points. Horizontal gray dashed lines indicate zero-temperature assigned to the different samples of the composition series $Nb_{1-y}Fe_{2+y}$.

the SDW state followed by a 1st order transition into the FM state exactly matches our observations in iron-rich $Nb_{0.985}Fe_{2.015}$.

We now turn to the behaviour at finite field. This is conveniently analysed at a fundamental level by comparing theoretical and experimental Arrott plots of $M^2$ vs. $H/M$. Outside the SDW phase we have

$$\frac{H}{M} = a + bM^2 \qquad\qquad \text{for} \quad P = 0 \qquad\qquad (2)$$

allowing us to extract $a(T)$ as well as $b(T)$ as the intercept and slope, respectively. Inside the SDW phase, i.e. for $P \neq 0$, this modifies the equation of state to $H = (a+\eta P^2)M+bM^3$ while at the same time minimizing the free energy with respect to $P$ gives $P^2 = -\frac{\alpha}{\beta} - \frac{\eta}{\beta}M^2$ Substituting this into the equation of state results in a modified expression for the Arrott plot within the SDW phase.

$$\frac{H}{M} = \underbrace{\left(a - \frac{\alpha\eta}{\beta}\right)}_{a^\star} + \underbrace{\left(b - \frac{\eta^2}{\beta}\right)}_{b^\star} M^2 \qquad\qquad \text{for} \quad P \neq 0 \qquad\qquad (3)$$

10

Thus, we expect a different slope and intercept in the SDW phase with $a^\star(T)$ bifurcating from $a(T)$ and $b^\star(T)$ jumping at $T_N$.

In Figs. 3 (b) and (f) we analyse the high- and low-field parts of the Arrott plots for NbFe$_2$ and Nb$_{0.985}$Fe$_{2.015}$ according to eqs. (2) and (3). Indeed, the slope $b^\star(T)$ extracted from the low-field part of the Arrott plot changes discontinuously from a positive value $b^\star = b$ outside the SDW phase to a negative value $b^\star \neq b$ inside the SDW phase. The temperature dependence of the extracted parameters in Figs. 3(c), (d), (g), and (h) agree with the expectations for a Landau theory for NbFe$_2$, Nb$_{0.985}$Fe$_{2.015}$, and Nb$_{1.01}$Fe$_{1.99}$ (not shown): (i) $b$ remains positive at all temperatures, (ii) $a$ has a strong temperature dependence, (iii) $a$ and $a^\star$ bifurcate at $T_N$, (iv) $b^\star$ changes discontinuously at $T_N$.

The high-field Arrot-plot intercept $a(T)$ (Figs. 3(c) and (g)) crosses through zero at an intermediate temperature $T_0 < T_N$ which indicates the underlying ferromagnetic instability. Ferromagnetism does not set in at $T_0$, because it has been preempted by SDW order at $T_N$, but instead a first order ferromagnetic transition occurs at a lower temperature $T_c < T_0$.

Considering next the shape of $M(H)$ isotherms on crossing the SDW phase boundary at constant $T$ yields two regimes within the two-order parameter model (eqs. 2 and 3) [29]. At low temperatures $M(H)$ is predicted to evolve discontinuously through the phase boundary whilst at high temperatures $M(H)$ evolves continuously. This implies that the phase boundary between the SDW state and the finite field paramagnetic state is expected 1st order and 2nd order at low and high temperatures with the two regimes separated by a tricritical point of divergent susceptibility at the maximum critical field of the SDW phase (cf. Fig. 4). This separation into a 1st and 2nd order regime of the SDW phase boundary entirely matches our observations in iron-rich Nb$_{0.985}$Fe$_{2.015}$ including the presence of a tricritical point with strongly enhanced susceptibility as discussed above (Fig. 2). For stoichiometric NbFe$_2$ and niobium-rich Nb$_{1.01}$Fe$_{1.99}$ only parts of the predicted phase diagram are accessible as indicated by the horizontal lines in Fig. 4: In NbFe$_2$ we observe the 2nd order upper phase boundary of the SDW phase and the tricritical point with a cut-off just below $T^\star$ whilst in Nb$_{1.01}$Fe$_{1.99}$ only the top part of the SDW phase is observed with a cut-off just below $T_N$.

Our findings are summarized in the global $H$-$T$-$y$ phase diagram in Fig. 5, which illustrates that the accessible part of the schematic phase diagram (Fig. 4) shrinks with increasing Nb content. The global phase diagram also illustrates the decrease of $T_0$ as the composi-
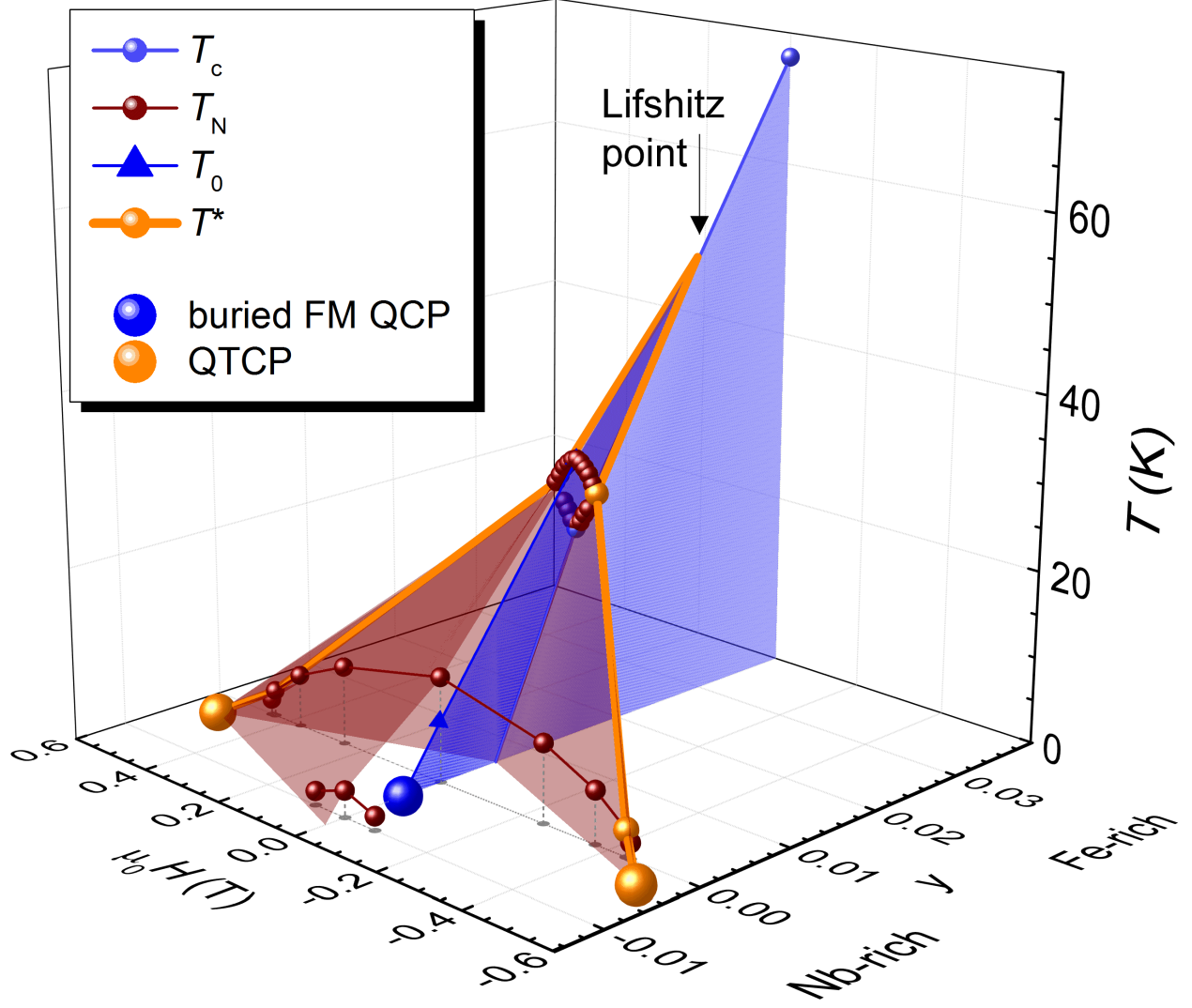
FIG. 5. Overall composition–magnetic field–temperature phase diagram for the $Nb_{1-y}Fe_{2+y}$ system. The underlying ferromagnetic transition temperature $T_0$ is extracted from $a(T_0) = 0$ (cf. Figs. 3(c) and (g)). The phase boundaries of the SDW and FM phase are obtained from the magnetization and susceptibility measurements as shown in Figs. 1, 2, and 3. The position of the avoided ferromagnetic QCP (blue ball) and the QTCPs (orange ball) are highlighted.

tion is varied from Fe-rich towards Nb-rich and that $T_0$ extrapolates to zero temperature at $y \approx -0.004$ and $H = 0$. This marks the avoided FM QCP buried inside a dome formed by the SDW phase. The intrinsic tendency of clean metallic systems to avoid a FM QCP either by changing the nature of the phase transition from 2nd order to 1st order or by developing competing SDW magnetic order has long been noted [2, 14, 16, 32]. Our observation of emergent SDW order enveloping the preempted FM QCP represents the first example of

the latter scenario among itinerant magnets, complementing the recent report of emergent helical order in the local moment system PrPtAl [20].

In addition to the buried FM QCP the global phase diagram (Fig. 5) reveals another important insight, the presence of quantum tricritical points (QTCPs): Finite-temperature tricritical points have been located for iron-rich $Nb_{0.985}Fe_{2.015}$ at $T^\star \approx 28\,K$ and for stoichiometric $NbFe_2$ at $T^\star \approx 3\,K$. This demonstrates that the tricritical points can be suppressed to zero temperature leading to QTCPs. Based on a smooth interpolation we estimate the location of the QTCPs at $(y \simeq -0.003, \pm\mu_0 H \simeq 0.5\,T, T = 0)$.

A divergent uniform susceptibility is not only expected within the two-order-parameter description above [29] but also within a self-consistent spin-fluctuation theory for antiferromagnetic order in itinerant systems [3]. The divergent uniform susceptibility near the QTCP causes strong FM fluctuations which may contribute to the logarithmic divergence of the specific heat observed near the SDW QCP at $(y \simeq -0.01, H = 0, T = 0)$ [9]. Indeed, recent theoretical work suggests that the finite temperature behaviour at an SDW QCP may be dominated by FM fluctuations of a nearby FM QCP above a crossover temperature that is different for different physical quantities [33]. In $NbFe_2$, we have a QTCP with FM fluctuations. At the nearby SDW QCP these FM fluctuations can produce $C/T \propto \log(T)$ above a low-lying crossover temperature specific to the heat capacity, whereas the corresponding crossover for resistivity may be higher, such that the signatures of SDW QCP are retained in $\rho(T)$ at low $T$.

Analysing our experimental results in newly available single crystals of the band magnet $NbFe_2$ and its iron-rich composition series in terms of a simple but powerful two order-parameter Landau theory has brought to light a new generic phase diagram for the vicinity of the FM QCP in clean metallic systems: (i) the FM QCP is enveloped by a dome of emergent SDW order, (ii) divergent $\chi$ is shifted to tricritical points at finite field, (iii) the line of tricritical points terminates at finite field at zero temperature, generating a QTCP. The coincidence of multiple phase boundaries and critical points may underlie the experimental observation that $C/T$ follows the $\log(T)$ behaviour characteristic of a FM QCP, whereas $\rho(T)$ displays the $T^{3/2}$ power law expected near an SDW QCP [9].

The identification of generic QTCPs in $NbFe_2$ opens up the new phenomenon of quantum tricriticality for experimental studies in a whole class of systems with buried or avoided FM QCP. This provides a fresh perspective on other materials with the same universality,

including prototypical heavy-fermion materials [3, 34], in which multiple and competing low-energy scales have in the past prevented the detection of a QTCP and obscured the investigation of its consequences.

## III.  MATERIALS AND METHODS

Samples from the composition series $Nb_{1-y}Fe_{2+y}$ with $-0.005 < y < 0.015$ were grown in an adapted, UHV-compatible mirror furnace from polycrystalline ingots prepared by radio-frequency induction melting, as described previously [35]. Single crystal grains were selected and oriented by x-ray and neutron diffraction. Magnetic and resistivity measurements were carried out on a Quantum Design PPMS. Thermal expansion measurements made use of a custom-designed dilatometry insert for the PPMS [36].

## IV.  DATA AVAILABILITY

All data needed to evaluate the conclusions in the paper are present in the paper, the Supplementary Materials and the Data repository at the University of Cambridge and can be download from https://www.repository.cam.ac.uk/handle/xxxx/xxxxx. Additional data related to this paper may be requested from the authors.

---

[1] Löhneysen, H. v., Rosch, A., Vojta, M. & Wölfle, P.  Fermi-liquid instabilities at magnetic quantum phase transitions. *Rev. Mod. Phys.* **79**, 1015–1075 (2007).

[2] Brando, M., Belitz, D., Grosche, F. M. & Kirkpatrick, T. R. Metallic Quantum Ferromagnets. *Review of Modern Physics* **88**, 025006 (2016).

[3] Misawa, T., Yamaji, Y. & Imada, M. $YbRh_2Si_2$: Quantum Tricritical Behavior in Itinerant Electron Systems. *J. Phys. Soc. Japan* **77**, 093712 (2008).

[4] Moriya, T. *Spin Fluctuations in Itinerant Electron Magnetism* (Springer, New York, 1985).

[5] Lonzarich, G. G.  The magnetic electron. In *Electron* (ed. Springford, M.) (Cambridge University Press, Cambridge, England, 1997).

[6] Pfleiderer, C., Julian, S. R. & Lonzarich, G. G. Non-Fermi-liquid nature of the normal state of itinerant- electron ferromagnets. *Nature* **414**, 427–430 (2001).

[7] Takashima, S. *et al.* Robustness of non-Fermi-liquid behavior near the ferromagnetic critical point in clean ZrZn$_2$. *J. Phys. Soc. Jpn.* **76**, 043704 (2007).

[8] Smith, R. P. *et al.* Marginal breakdown of the Fermi-liquid state on the border of metallic ferromagnetism. *Nature* **455**, 1220–1223 (2008).

[9] Brando, M. *et al.* Logarithmic fermi-liquid breakdown in NbFe$_2$. *Phys. Rev. Lett.* **101**, 026401 (2008).

[10] Belitz, D., Kirkpatrick, T. R. & Vojta, T. First order transitions and multicritical points in weak itinerant ferromagnets. *Phys. Rev. Lett.* **82**, 4707–4710 (1999).

[11] Pfleiderer, C., MeMullan, G. & Lonzarich, G. Critical behaviour at the transition from a magnetic to a nonmagnetic metallic state in MnSi as a function of hydrostatic pressure. *Phys. B Condens. Matter* **199-200**, 634–636 (1994).

[12] Pfleiderer, C., McMullan, G. J., Julian, S. R. & Lonzarich, G. G. Magnetic quantum phase transition in MnSi under hydrostatic pressure. *Phys. Rev. B* **55**, 8330–8338 (1997).

[13] Uhlarz, M., Pfleiderer, C. & Hayden, S. M. Quantum Phase Transitions in the Itinerant Ferromagnet ZrZn$_2$. *Phys. Rev. Lett.* **93**, 256404 (2004).

[14] Belitz, D., Kirkpatrick, T. R. & Vojta, T. Nonanalytic behavior of the spin susceptibility in clean Fermi systems. *Phys. Rev. B* **55**, 9452–9462 (1997).

[15] Chubukov, A. V., Pepin, C. & Rech, J. Instability of the quantum-critical point of itinerant ferromagnets. *Phys. Rev. Lett.* **92**, 147003 (2004).

[16] Conduit, G. J., Green, A. G. & Simons, B. D. Inhomogeneous Phase Formation on the Border of Itinerant Ferromagnetism. *Phys. Rev. Lett.* **103**, 207201 (2009).

[17] Pedder, C. J., Krüger, F. & Green, A. G. Resummation of fluctuations near ferromagnetic quantum critical points. *Phys. Rev. B* **88**, 165109 (2013).

[18] Moroni-Klementowicz, D. *et al.* Magnetism in Nb$_{1-y}$Fe$_{2+y}$: Composition and magnetic field dependence. *Phys. Rev. B* **79**, 224410 (2009).

[19] Taufour, V. *et al.* Ferromagnetic Quantum Critical Point Avoided by the Appearance of Another Magnetic Phase in LaCrGe$_3$ under Pressure. *Phys. Rev. Lett.* **117**, 037207 (2016).

[20] Abdul-Jabbar, G. *et al.* Modulated magnetism in PrPtAl. *Nat. Phys.* **11**, 321–327 (2015).

[21] Kotegawa, H. *et al.* Pressure-Temperature-Magnetic Field Phase Diagram of Ferromagnetic Kondo Lattice CeRuPO. *J. Phys. Soc. Japan* **82**, 123711 (2013).

[22] Lausberg, S. *et al.* Avoided Ferromagnetic Quantum Critical Point: Unusual Short-Range Ordered State in CeFePO. *Phys. Rev. Lett.* **109**, 216402 (2012).

[23] Lausberg, S. *et al.* Doped $YbRh_2Si_2$ : Not Only Ferromagnetic Correlations but Ferromagnetic Order. *Phys. Rev. Lett.* **110**, 256402 (2013).

[24] Shiga, M. & Nakamura, Y. Magnetic-Properties Of Stoichiometric And Off-Stoichiometric $NbFe_2$. *J. Phys. Soc. Jpn.* **56**, 4040–4046 (1987).

[25] Yamada, Y. & Sakata, A. Weak Antiferromagnetism In $NbFe_2$. *J. Phys. Soc. Jpn.* **57**, 46–47 (1988).

[26] Crook, M. R. & Cywinski, R. Magnetic transitions in $Nb_{1-y}Fe_{2+y}$. *J. Magn. Magn. Mater.* **140-144**, 71–72 (1995).

[27] Rauch, D. *et al.* Spectroscopic study of the magnetic ground state of $Nb_{1-y}Fe_{2+y}$. *Phys. Rev. B* **91**, 174404 (2015).

[28] Niklowitz, P. G. *et al.* Ultra-small moment incommensurate spin density wave order masking a ferromagnetic quantum critical point in $NbFe_2$. *arXiv:1704.08379 [cond-mat.str-el]* (2017).

[29] Moriya, T. & Usami, K. Coexistence of Ferromagnetism and Antiferromagnetism and Phase-Transitions in Itinerant Electron-Systems. *Solid State Commun.* **23**, 935–938 (1977).

[30] Lawrie, I. D. & Sarbach, S. *Phase Transitions and Critical Phenomena*, vol. 9, chap. Theory of Tricritical Points, 1–163 (Academic Press, London, 1984).

[31] Rost, A. W., Perry, R. S., Mercure, J.-F., Mackenzie, A. P. & Grigera, S. A. Entropy Landscape of Phase Formation Associated with Quantum Criticality in $Sr_3Ru_2O_7$. *Science* **325**, 1360–1363 (2009).

[32] Vojta, T., Belitz, D., Kirkpatrick, T. & Narayanan, R. Quantum critical behavior of itinerant ferromagnets. *Ann. Phys.* **8**, 593–602 (1999).

[33] Oliver, G. T. & Schofield, A. J. Quantum Multicriticality. *arXiv:1506.03021 [cond-mat.str-el]* (2015).

[34] Misawa, T., Yamaji, Y. & Imada, M. Spin Fluctuation Theory for Quantum Tricritical Point Arising in Proximity to First-Order Phase Transitions: Applications to Heavy-Fermion Systems, $YbRh_2Si_2$, $CeRu_2Si_2$ , and $\beta$-$YbAlB_4$. *J. Phys. Soc. Japan* **78**, 084707 (2009).

[35] Friedemann, S. *et al.* Ordinary and intrinsic anomalous Hall effects in $Nb_{1-y}Fe_{2+y}$. *Phys. Rev. B* **87**, 024410 (2013).

[36] Küchler, R., Bauer, T., Brando, M. & Steglich, F. A compact and miniaturized high resolution capacitance dilatometer for measuring thermal expansion and magnetostriction. *Rev. Sci. Instrum.* **83**, 095102 (2012).

## V.   ACKNOWLEDGEMENT

# Supplementary Materials to
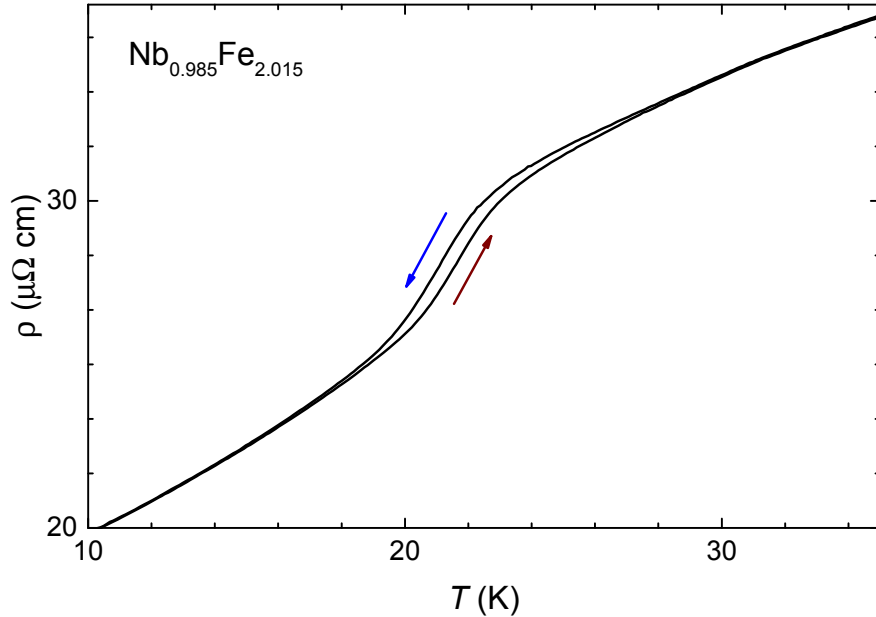# "Buried ferromagnetic quantum critical point in single-crystal NbFe$_2$"

FIG. S1. Hysteresis at the FM transition in the resistivity for $Nb_{0.985}Fe_{2.015}$. Arrows indicate the direction of the temperature sweep.

## I. PHASE TRANSITION CHARACTERISTICS IN $Nb_{0.985}Fe_{2.015}$

The zero-field transition into the ferromagnetic state of $Nb_{0.985}Fe_{2.015}$ shows clear hysteresis as evident from resistivity measurements in Fig. S1 and the susceptibility (Fig. 1(a)). This implies a first-order transition at $T_c$.

In finite field, hysteresis is present below $T^\star$ at the low-temperature transition of the SDW phase only as observed in the susceptibility (Fig. S2(a)). This implies a first order transition for $T < T^\star$ and a second order transition for $T > T^\star$ with a tricritical point at $(H^\star, T^\star)$. In addition, we find a peak in the imaginary part of the AC susceptibility $\chi''(T)$ along the low-temperature boundary of the SDW phase (Fig. S2(b)). Indeed this peak becomes more pronounced on the approach of $H^\star$ indicative of the 1st order becoming weaker and thus promoting strong dissipation. This trend culminates in a strong enhancement of $\chi''(T)$ right at $H^\star$ for temperatures below $T^\star$ and suggests ultimate proximity to a tricritical point with fluctuations in the uniform susceptibility.

Figure S3 highlights the enhancement of the uniform susceptibility at $(H^\star, T^\star)$. These divergent fluctuations at zero wavevector together with divergent fluctuations at finite wavevector which are implied by the 2nd order nature of the SDW transition at $T^\star$ charac-
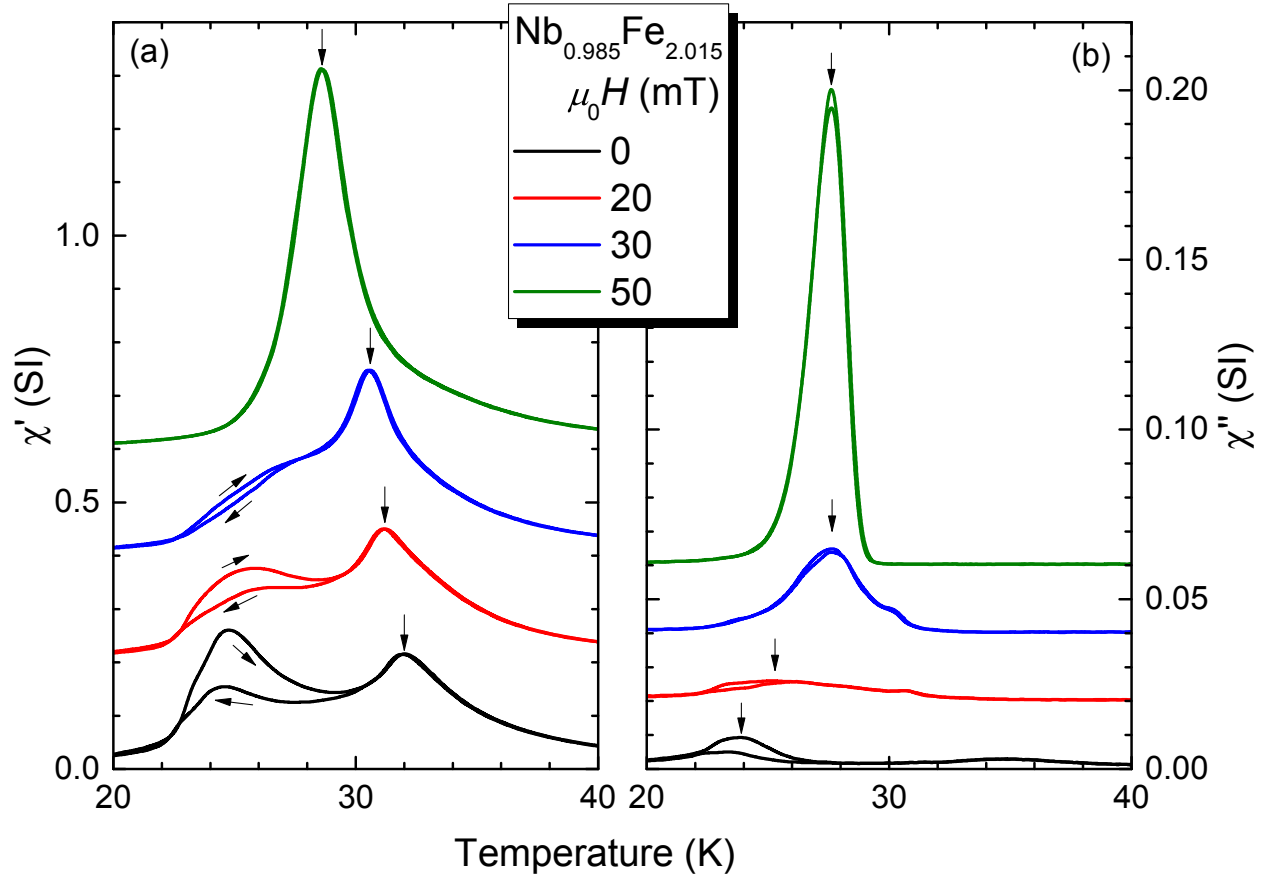
FIG. S2. Hysteresis in temperature sweeps of the AC susceptibility real $\chi'(T)$ and imaginary part $\chi''(T)$. Vertical arrows in (a) and (b) indicate the upper and lower transition of the SDW state, respectively. Arrows around the lower transition in (a) indicate the direction of sweeping the temperature. Data are offset by 0.2 (a) and 0.02 (b) for clarity.

terise the tricritical point at $(H^\star, T^\star)$.
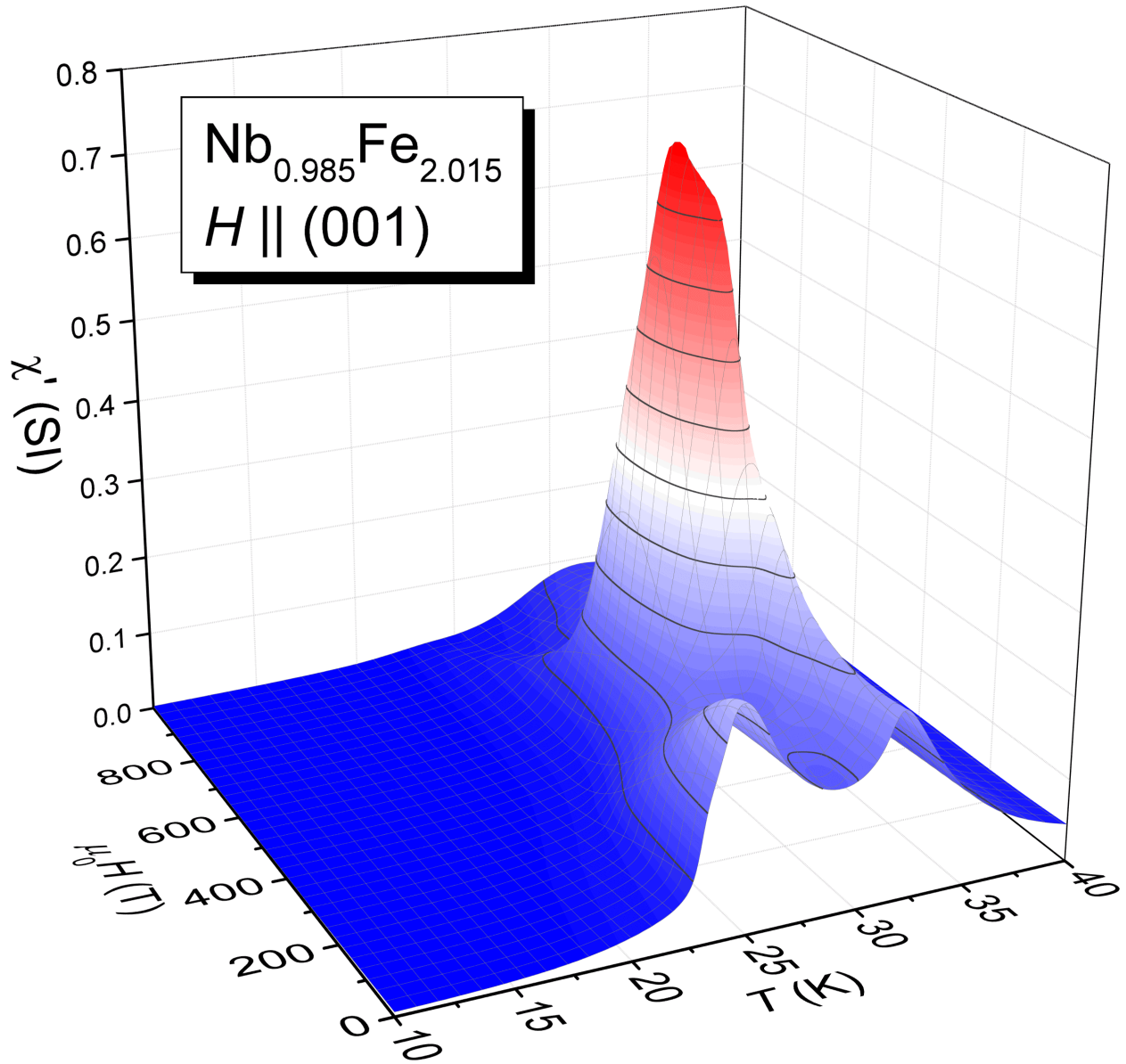
FIG. S3.   Magnetic susceptibility map for iron-rich $Nb_{0.985}Fe_{2.015}$.  The three-dimensional representation was constructed from warming temperature sweeps after field cooling.